Chemical Science

ROYAL SOCIETY OF CHEMISTRY

EDGE ARTICLE

View Article Online
View Journal

Cite this: DOI: 10.1039/d5sc08870d

All publication charges for this article have been paid for by the Royal Society of Chemistry

Leveraging the redox activities of cerium and dibenzotetrathiafulvalene to discover a photo-responsive magnetic material

Himanshu Gupta,[a] Ethan P. Shapera,[b] Xiaojuan Yu,[b] Xiaoyu Wang,[b] Patrick W. Smith,[c] Pragati Pandey,[d] Michael R. Gau,[a] Stefan G. Minasian,*[c] Eva Zurek,*[b] Jochen Autschbach,*[b] James M. Kikkawa*[e] and Eric J. Schelter*[afg]

Stimuli-responsive changes in lanthanide-based materials are a promising research direction. In this study, $[DBTTF]_4[Ce_2Cl_{10}]$ DBTTF = dibenzotetrathiafulvalene (**1**) was synthesized by a light-induced crystallization, where photo-oxidation of DBTTF enables formation of the cerium dimer $[Ce_2Cl_{10}]^{4-}$. Intermolecular interactions between the stacked organic units of the crystal result in charge transfer bands in the visible-NIR (near-infrared) region, evident in the solid-state absorption spectrum upon comparison with the solution spectrum. The assignments of the sublattice oxidation states were made with single-crystal X-ray diffraction (SC-XRD) structural characterization, Raman spectroscopy, X-ray absorption spectroscopy, and magnetometry. Continuous 532 nm laser irradiation of the microcrystalline solid modulates the redox states in **1**, leading to ~40% reduction in the observed magnetization at 2 K. Density functional theory PBE+*U*/HSE06 band structure calculations predict Mott insulating behavior in **1**, with a bandgap of 0.54/0.81 eV, and further support the conjecture that the observed photo-induced change in magnetization results from electron transfer from the $[Ce_2Cl_{10}]^{4-}$ anions to the π-stacked $[DBTTF]_2^{2+}$ organic dimer subunits. An enhancement in conductivity is similarly observed upon 532 nm irradiation, determined by single-crystal transport measurements. The findings reveal that photo-responsive lanthanide-based materials can be achieved by integration of redox-active organic moieties with redox-active lanthanide cations for the realization of switchable, photo-magnetic materials.

Received 13th November 2025
Accepted 11th March 2026

DOI: 10.1039/d5sc08870d

rsc.li/chemical-science

Introduction

Molecule-based lanthanide materials and their electronic, optical, and magnetic properties have gained attention for advancing fundamental studies of f-electron behavior and for manifesting multi-functional materials.[1–4] Reports on temperature-induced valence tautomerization in $[SmI_2(pyz)_3]$, intermediate valency in $[(C_5Me_5)_2Yb(bipy)]$, and photon-induced covalency in $[Sm(C_9H_9)_2]$ have provided recent notable steps forward.[5–8] There are prospects for control over these formal oxidation states, and their associated materials properties, through external stimuli such as light, temperature, pressure *etc.*[9–11]

Molecular cerium compounds such as $[Ce(COT)_2]$ COT^{2-} = $C_8H_8^{2-}$ have been extensively investigated *via* spectroscopy and computations, indicating Kondo singlet behavior of f-electrons interacting with delocalized π-electrons through strong static electron correlations.[12–14] These attributes offer opportunities to develop novel cerium-based extended molecular materials that allow for the study of the stimuli effects on the local and global electronic structure for next-generation electronic materials. In this context, we recently reported redox assembly of cerium compounds including a mixed-valent complex $(Cp_3Ce^{IV})_2$(-TCNQ)$(Ce^{III}Cp_3)_2$ TCNQ = tetracyanoquinodimethane, Cp^- = cyclopentadienyl, and a fullerene-based material $[(C_5Me_4H)_3$-$Ce]_2 \cdot C_{60}$.[15,16] Emergent Mott insulator behavior was promoted in the latter through partial charge transfer interactions.

DBTTF (dibenzotetrathiafulvalene) and related fulvalenes form charge transfer stacked materials comprising an oxidized tetrathiafulvalene ($TTF^{\bullet+}$) core that are well-established to

[a]*Vagelos Laboratory for Energy Science and Technology, Department of Chemistry, University of Pennsylvania, Philadelphia, PA 19104, USA. E-mail: schelter@sas.upenn.edu*

[b]*Department of Chemistry, University at Buffalo, State University of New York, Buffalo, NY 14260, USA. E-mail: ezurek@buffalo.edu; jochena@buffalo.edu*

[c]*Chemical Sciences Division, Lawrence Berkeley National Laboratory, Berkeley, CA 94720, USA. E-mail: sgminasian@lbl.gov*

[d]*Institut des Sciences et Ingénierie Chimiques, École Polytechnique Fédérale de Lausanne (EPFL), CH-1015 Lausanne, Switzerland*

[e]*Department of Physics and Astronomy, University of Pennsylvania, Philadelphia, PA 19104, USA. E-mail: kikkawa@physics.upenn.edu*

[f]*Department of Earth and Environmental Science, USA*

[g]*Department of Chemical and Biomolecular Engineering, University of Pennsylvania, Philadelphia, PA 19104, USA*

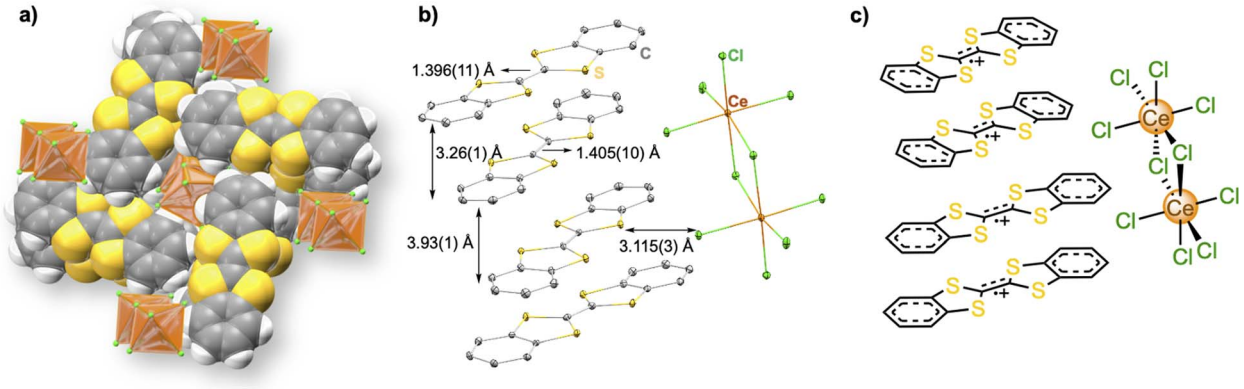

Fig. 1 (a) Structural fragment of **1** showing an extended structure with 1D stacks of $DBTTF^{\bullet+}$ in a space filling model. (b) Thermal ellipsoid plot of **1** at 30% probability level with appropriate distance, Ce–Cl_{term} distance are 2.727(2), 2.7133(19), 2.7027(17) and 2.734(2) Å, Ce–$Cl_{bridging}$ distance are relatively elongated 2.8501(16) and 2.9140(19) Å; hydrogen atoms are omitted for clarity. (c) Chemdraw depiction of **1** showing bi-octahedral cerium dimer $[Ce_2Cl_{10}]^{4-}$ with $DBTTF^{\bullet+}$ stacks.

promote the occurrence of conducting and magnetic behavior.[17–20] These properties emerge from partial band filling due to incomplete oxidation of sulfur p-orbitals in extended stack structures. However, stimuli-induced changes in physical properties for such stacked materials upon combination with lanthanides have remained unexplored. Previous studies by our group demonstrated that photoirradiation can trigger electron transfer processes in $[CeCl_6]^{3-}$ to reduce organic compounds.[21] Herein, we extended this concept by inducing changes in electronic and magnetic properties by photoexcitation. In this work, we have shown formation of a novel cerium dimer to form the molecular material $[DBTTF]_4[Ce_2Cl_{10}]$ (**1**) with $DBTTF^{\bullet+}$ stacks (Fig. 1). We have further explored photo-effects on the modulation of redox states and magnetic properties of this newly synthesized material, accompanied by enhanced conductivity.

Results and discussion

Synthesis and structural characterization

A previous report has described the photochemical oxidation of TTF and related analogues in the presence of carbon tetrachloride (CCl_4), which crystallizes as mixed-valent species $(TTF)Cl_{0.68}$.[22] Photoinduced oxidation of substituted thiafulvalenes and other redox-active organic molecules in halocarbon solvents has also been reported previously and provide relevant mechanistic precedent.[23–27] When trivalent metal chlorides are added to the photo-crystallization reaction mixture, they recombine with these *in situ* generated TTF^+ chloride species and produce stacked materials of the formula $(TTF)_3[MCl_6]$.[28] We have successfully adopted this photochemical methodology (Scheme 1) for the synthesis of **1** by using neutral DBTTF and $CeCl_3$ precursors (see SI for synthetic details). A yellow CCl_4/CH_3CH_2OH solution of neutral DBTTF and $CeCl_3$ turned dark green immediately upon irradiation, characteristic of $DBTTF^{\bullet+}$ formation in solution.[29] *In situ* generated $DBTTF^{\bullet+}$ chloride evidently combines with $CeCl_3$ to enable formation of a unique cerium dimer, $[Ce_2Cl_{10}]^{4-}$, with octahedral cerium cations bridged by two chloride ligands, which forms purple-black microcrystals from the mixture in 36.8% yield. Single crystal X-ray diffraction analysis confirmed the formation of **1** (*vide infra*). Powder X-ray diffraction and elemental analysis further confirmed the bulk purity of the crystalline material (Fig. S3).

Compound **1** crystallizes in $P2_1/n$ space group with stacked $DBTTF^{\bullet+}$ units and dimeric cerium chlorides in independent alternating layers (Fig. 1). The $[Ce_2Cl_{10}]^{4-}$ anion is reminiscent of our previous studies of face-sharing bi-octahedral cerium chloride dimers comprising three bridging chlorides instead of two.[21] Terminal Ce–Cl bond lengths are 2.727(2), 2.7133(19), 2.7027(17) and 2.734(2) Å, which are consistent with the +3 oxidation state assignment of the cerium cation in **1**. The bridging chloride ligands show relatively elongated Ce–Cl bond lengths of 2.8501(16) and 2.9140(19) Å. The crystal structure also revealed one-dimensional slip-stacked units of $DBTTF^{\bullet+}$. The closest C···C distances between each $DBTTF^{\bullet+}$ stacked unit are 3.26(1) Å and 3.93(1) Å, signifying an alternating, strong π-dimer formation.[30] The central C–C bond lengths in successive $DBTTF^{\bullet+}$ units are 1.396(11) and 1.405(10) Å, which is consistent with the radical cation form of DBTTF in **1**.[20] The closest S···Cl

Previous Work : Redox Inactive Metal (M= In, Sb)

$$MCl_3 \xrightarrow[h\nu\ (370\ nm),\ 3h,\ CCl_4]{TTF} [TTF]_3[M^{III}Cl_6]$$

This Work : Redox Active Metal $Ce^{III/IV}$

$$CeCl_3 \xrightarrow[h\nu\ (370\ nm),\ 3h,\ CCl_4]{DBTTF} [DBTTF]_4[Ce^{III}_2Cl_{10}]$$

(1)

Scheme 1 Previous work describing photo-oxidation of TTF to form TTF chloride and further recombination to form metal-TTF material; this work showing the recombination of *in situ* generated TTF analogue DBTTF chloride under irradiation to form **1**.

distance is 3.115(3) Å, which is shorter than the sum of the van der Waals radii of sulfur and chlorine (≈3.55 Å),[31] suggesting that the intermolecular charge transfer interactions between organic and inorganic units play an important role in stabilizing the material.[28]

Control reactions were performed to investigate the participation of each component in the photo reaction (Table S1). Excluding CCl_4 from the reaction mixture did not yield any precipitate and the color of the reaction remained yellow throughout the 3 h interval, indicating no oxidation of DBTTF. This observation confirms that the chloride radicals originate from CCl_4. Excluding light from the reaction mixture also did not yield any precipitate and the reaction color remained yellow. In the absence of $CeCl_3$, the reaction mixture became dark green upon irradiation due to the formation of $DBTTF^{\bullet+}$; however, no precipitate was observed even after an extended period of irradiation, presumably due to the solubility of [DBTTF]Cl. Surprisingly, reactions performed with $LaCl_3$ instead of $CeCl_3$ did not yield any precipitate, despite the similarity in size of La^{3+} (1.03 Å) and Ce^{3+} (1.01 Å) cations. Overall, this photochemical method is experimentally demonstrated for cerium with DBTTF, as well as faster and more efficient compared to the typical electrocrystallization methods that require weeks to months to synthesize charge transfer materials.[20] Additionally, control experiments show that photooxidation of DBTTF to $DBTTF^{\bullet+}$ occurs in CCl_4 under irradiation even in the absence of cerium salts. However, under these conditions no crystalline material can be isolated. The role of cerium is therefore not to generate the radical cation but to enable crystallization by formation of the dimeric $[Ce_2Cl_{10}]^{4-}$ counter-anion that stabilizes the $DBTTF^{\bullet+}$ sublattice in the solid state. Having demonstrated effective synthesis of **1**, we next turned to its characterization.

Spectroscopic characterization

Raman spectroscopy is used to assign formal oxidation states in fulvalene-based materials.[32,33] Among all vibrational modes, the C=C symmetrical stretch is characteristic of the redox state of the TTF core.[34] The main feature of neutral DBTTF at 1553 cm^{-1} significantly shifts to a lower frequency (~1400 cm^{-1}) due to oxidation.[35] In **1**, this band appears at 1407 cm^{-1}, indicative of $DBTTF^{\bullet+}$ (Fig. S4). The cerium oxidation state in **1** was further confirmed by L_3-edge X-ray absorption near-edge structure (XANES) spectroscopy (Fig. S1). For intermediate-valent or Ce^{IV} complexes, Ce L_3-edge XANES spectra (Ce $2p_{1/2} \rightarrow 5d_{3/2}$) typically consist of two features.[12,36,37] The relative weights of the two peaks are often used to evaluate 4f electron density at Ce using a configuration interaction (CI) model.[38–40] Using the CI model, the lower energy feature is attributed to a $2p^54f^15d^1$ final configuration and the higher energy feature is attributed to a $2p^54f^05d^1$ final configuration, with intensities that are reflective of the relative weight of $4f^1$ and $4f^0$ configurations in the ground state. The XANES of **1** consists of a strong peak in the rising edge at 5724 eV, in the region commonly observed for trivalent Ce complexes. There is a second, broader feature centered around 5734 eV, near the energy commonly observed for transitions into the $2p^54f^05d^1$ excited state. However, the large width of this feature is atypical for bound-state transitions, and more consistent with the onset of extended X-ray absorption fine structure (EXAFS). This interpretation is supported by FDMNES computations. FDMNES computations are effective for EXAFS simulation, however, because the method is single reference, they do not capture the multiplet structure observed in the Ce L_3-edge XANES of intermediate-valent or Ce^{IV} complexes. The appearance of this feature in the FDMNES simulated Ce L_3-edge spectrum of **1** supports its assignment as an EXAFS feature. Taken together, the Raman and L_3-edge XANES data support ground-state $DBTTF^{\bullet+}$ and Ce^{III} oxidation states.

To understand the optical properties of **1**, electronic absorption data were collected in both the solution state (methanol) and the solid state (Fig. 2a). In solution, **1** is well-dissolved so that individual $DBTTF^{\bullet+}$ and Ce^{III} centers are isolated, leading to sharp and well-defined absorption bands at 248, 310, 341, 423, 441, and 581 nm, corresponding to the intrinsic electronic transitions of the $DBTTF^{\bullet+}$ and Ce^{III} cations.[41,42] In contrast, the solid-state spectrum of **1** presents pronounced broadening in absorption features compared to the solution state data. Evidently, the close packing of $DBTTF^{\bullet+}$ in **1** promotes strong intermolecular interactions in the solid state

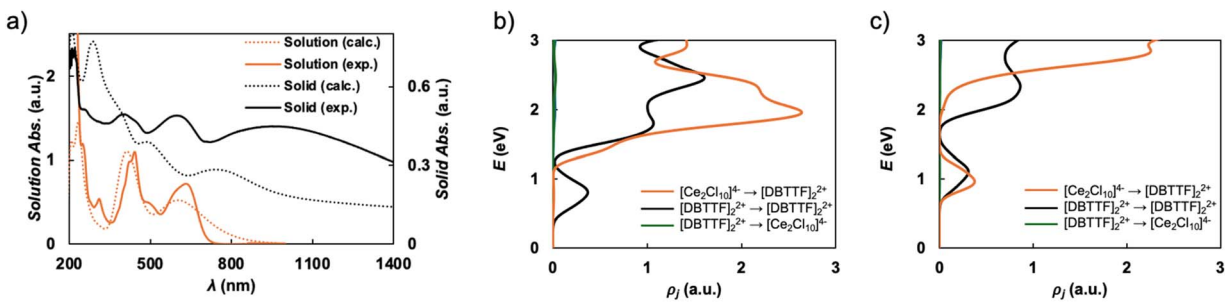

Fig. 2 (a) Calculated absorption spectra of a $DBTTF^{\bullet+}$; isolated monomer spectrum (dotted orange) obtained at the PBE/def2-SVPD level and periodic solid-state spectrum (dotted black) from PBC (periodic boundary conditions)-DFT method (with PBE+*U*). Molecular structure taken from the experimental crystal structure (H positions optimized). The experimental spectra of **1** in solution and the solid state are shown for comparison (solid orange and solid black), respectively. (b and c) Joint densities of states (JDOS, ρ_J) for optical transitions of electrons from occupied to unoccupied bands in **1**, colored according to orbitals involved in the excitation, computed using (b) PBE+*U* and (c) HSE-06 exchange–correlation functional.

due to charge transfer interactions between adjacent DBTTF stacks and possibly between $DBTTF^{\bullet+}$ and Ce^{III} centers.

Computational analysis

Time-dependent (TD) density functional theory (DFT) calculations of the absorption spectrum of isolated $DBTTF^{\bullet+}$ and its dimer were carried out (see SI for computational details). The monomer calculations with a variety of functionals, including PBE (*vide infra*), reproduce the main peak structure of the solution-state spectrum of **1** and therefore support the assignment of isolated $DBTTF^{\bullet+}$ and Ce^{III} centers in solution (Fig. S14). These calculations also indicate that most of the absorption intensity in the solution of **1** arises from solvated $DBTTF^{\bullet+}$. Transitions localized at the Ce^{III} centers, in particular the transitions among the states of the $4f^1$ manifold, may also occur but are expected to have low intensity because of the approximate local octahedral coordination environment and the corresponding parity selection rule. Molecular TDDFT calculations of a singlet-coupled $DBTTF^{\bullet+}$ dimer likewise exhibit the three-main-peak structure seen below 700 nm in the experimental solid-state spectrum of **1** and additionally a broad peak at low energies (wavelengths >700 nm). These results suggest that much of the observed intensity for the solid is associated simply with transitions within $DBTTF^{\bullet+}$ and its dimer. However, additional calculations carried out with periodic boundary conditions (PBC) DFT for the crystal of **1**, which are discussed later, show crucial contributions to the spectrum from orbitals associated with the Ce^{III} centers.

Magnetic measurements

Bulk magnetic data on **1**, which has two types of spin centers, the Ce^{III} ions and $DBTTF^{\bullet+}$, was collected. The variable temperature magnetic susceptibility showed a value $\chi T = 1.29$ emu K mol^{-1} at 300 K and gradually decreased to 0.40 emu K mol^{-1} at 2 K (Fig. S6). In an ideal case, each Ce^{III} ion is expected to contribute one $4f^1$ unpaired electron with $\chi T = 0.8$ emu K mol^{-1} at 300 K while a free $DBTTF^{\bullet+}$ carries an $S = \frac{1}{2}$ spin. However, as evident by SC-XRD and solid-state absorption studies, the $DBTTF^{\bullet+}$ units are dimerized with strong π–π interactions, resulting in antiferromagnetically coupled spin pairs effectively canceling each other's spin. As a result, the measured magnetic properties, including the field-dependent magnetization that saturates at about $1.41\mu_B$ at 2 K, are dominated by the Ce^{III} centers (Fig. S6). For comparison, a free Ce^{III} ion ($4f^1$, $^2F_{5/2}$, $g_J = 6/7$) has an ideal saturation magnetization of $2.14\mu_B$ per ion, although significantly lower values are typically observed in molecular complexes due to crystal-field splitting and strong magnetic anisotropy.[43–46] The reduction in χT at low temperature is primarily attributed to crystal-field splitting and depopulation of excited m_J states within the $J = 5/2$ manifold of Ce^{III}, consistent with strong spin–orbit coupling in f^1 systems, any exchange coupling are expected to be very weak. Such bulk magnetism in charge transfer stacked materials with paramagnetic ions has been noted previously.[47–49] The organic stacked materials with oxidized TTF core stacks tend to show Pauli paramagnetism, masked by that response for metal cations with unpaired electrons.[43,50] PBC DFT calculations with PBE+*U*, as well as with the HSE-06 screened hybrid functional (Table S2), predict a net magnetic moment of 0.99 μ_B on each Ce atom, confirming the weak antiferromagnetic coupling between the Ce^{III} centers. Furthermore, they indicate Mott insulating behavior in **1**, whose bandgap is predicted to be 0.54/0.81 eV with PBE+*U*/HSE06.

Motivated by the known photo-reducing properties of Ce^{III} chlorides in solution,[33,51] we performed magnetic measurements under optical illumination with 532 nm light at 2*T* on the microcrystalline powder of **1** to modulate its redox state. Evidently, a photo-induced charge transfer occurs in **1** at lower temperatures. Considering the dark and irradiated conditions, the magnetic susceptibility is essentially unchanged in the high temperature regime. However, differences become significant below 15 K and are prominent at the lowest measured temperature of 2 K (Fig. 3). With the highest optical power density used, $I_o = 0.5$ mW mm^{-2}, the bulk magnetic moment is reduced by over 40% compared to its dark state value (Fig. 3 inset). Comparisons to the magnetic response of a control sample $(NEt_4)_3[CeCl_6]$ discourage the interpretation that the observed changes are due to heating, as no significant increase in the lattice temperature of $(NEt_4)_3[CeCl_6]$ was observed under identical excitation and measurement conditions (Fig. S8). The observed photo response of **1** is also sublinear in the incident power, which would be difficult to explain with heating (Fig. S7). The data may instead indicate that a significant fraction of Ce^{III} is being photo-oxidized to Ce^{IV} ($4f^0$, diamagnetic), resulting in lower susceptibility *via* conversion to a lower spin state due to loss of the 4f orbital angular momentum contribution. The curvature and saturation are very obviously different compared to the two *M vs. H* curves. There are only two factors that can explain the more linear form of the laser ON data. Either (a) higher spin temperature (heating), or (b) a conversion to a lower spin state along with a drop in M_{sat}, or some combination of (a) and (b). The contrasting photo-response with $(NEt_4)_3[CeCl_6]$ dissuades the heating scenario.

Transport measurements

Photoconductivity measurements were performed to detect if modulation in redox states was accompanied by a change in

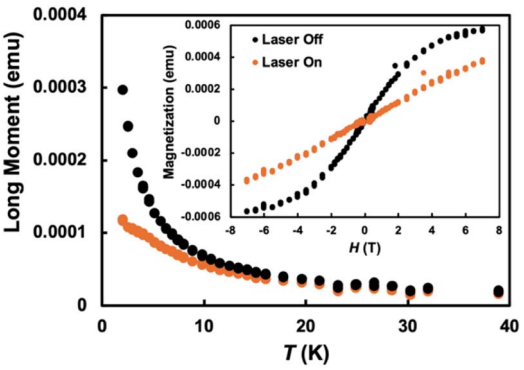

Fig. 3 Variable temperature magnetic susceptibility in laser off and on conditions at 2 Tesla. (Inset) Magnetic hysteresis loop recorded at 2 K in laser off and on ($I = I_o$) conditions.

conduction. Charge transport performed on single crystal samples of **1** in the dark shows the material is increasingly resistive at low temperature (Fig. S10). Thus, the temperature window for the measurement is restricted to 155 K and above. This behavior is consistent with the bulk magnetic data, showing charge carriers are localized on the Ce^{III} centers and $DBTTF^{\bullet+}$ carriers have strong π–π interactions that form Peierls dimers. Upon illumination with 532 nm light, however, a photo-induced charge transfer process is activated, leading to a drop in resistance. Fig. 4a shows the photo-resistive transients recorded at $T = 155$ K. Examination of the resistance drops for several temperatures indicate that heating is not the dominant source of the decreased resistance recorded here (Fig. S11). Instead, the data indicate photoexcitation of a charge transfer transition between localized and delocalized electronic states, consistent with the magnetometry data, which suggest the latter have a lower spin.

A sharp eye will notice that photoconductive transients saturate more slowly at lower powers. Modeling the data using an exponential rise, $\Delta R(1 - e^{-\Gamma t})$, we plot Γ in Fig. 4b, showing a proportionality to and eventually saturation with laser intensity I. The initial proportionality is easy to understand because the rate of charge transfer should be proportional to laser power. The saturation of the rate for the highest laser intensities can then be understood within a rate-equation approach to charge transfer where, for higher laser intensities, the equilibrium population imbalance increases the spontaneous recombination rate. Evidently, this photo-induced modulation of redox states leads to reorganization of the charge density along the molecular stacks: the partial oxidation of Ce^{III} to Ce^{IV} promotes partial reduction of $DBTTF^{\bullet+}$ to its neutral state forming mixed valent stacks that are well understood to promote enhanced conductivity.[52] Overall, photoconductivity in **1** is most consistent with a reversible, photo-induced charge transfer that increases the density of mobile charge carriers along the $DBTTF^{\bullet+}$ stacks.

The density of states (DOS) (Fig. S15) and joint density of states (JDOS) (Fig. 2b and c) from both PBE+U and HSE-06 PBC calculations support the interpretation of the experimental data, illustrating that light with a wavelength of 532 nm (2.33 eV) not only induces charge transfer interactions between adjacent DBTTF stacks, but also $[Ce_2Cl_{10}]^{4-} \rightarrow [DBTTF]_2^{2+}$ electronic excitations. These transitions are not impacted by the parity selection rule. Theoretical evidence for the presence of these types of excitations in solid **1** is obtained by determining that the relative energies between the DBTTF valence states comprising the conduction band and the occupied states projecting onto the $[Ce_2Cl_{10}]^{4-}$ dimers in the DOS encompass the laser energy. The JDOS counts the number of possible transitions to any unoccupied state that could occur for a particular photon energy, clearly showing that both $[DBTTF]_2^{2+} \rightarrow [DBTTF]_2^{2+}$, and $[Ce_2Cl_{10}]^{4-} \rightarrow [DBTTF]_2^{2+}$ excitations can occur at 2.33 eV. As such, the overall model of a photo-induced decrease in magnetization and increase in conductivity due to charge transfer between the inorganic and organic sublattices is supported by the periodic electronic structure calculations.

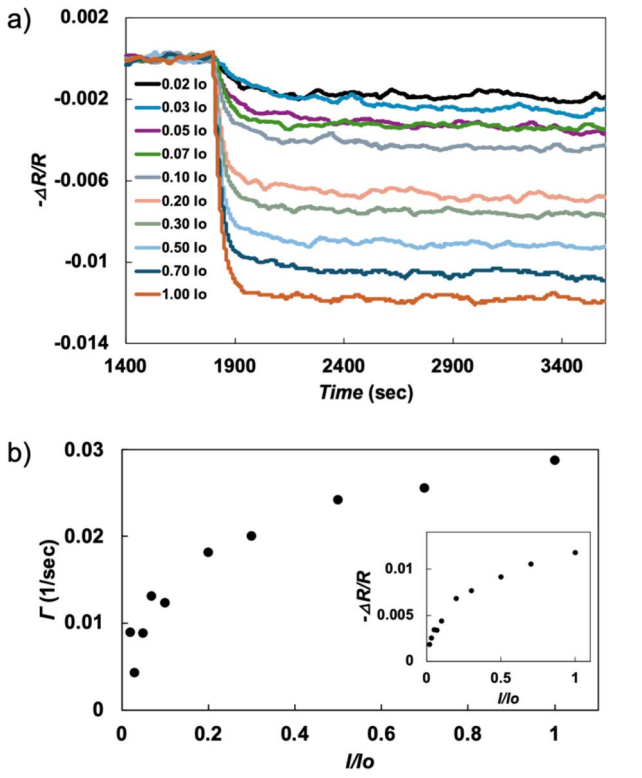

Fig. 4 (a) Photoconductive resistive transients in **1** for different degrees of laser power. (b) Power-dependent rise time for the measured data set. Data collected at $T = 155$ K.

Conclusions

We have demonstrated the design of a photo-responsive magnetic material by leveraging the interplay between a redox-active lanthanide ($Ce^{III/IV}$) and a redox-active organic species ($DBTTF^{0/\bullet+}$). An efficient and fast photo-induced crystallization of **1** facilitates discovery of new, molecule-based charge transfer materials. The enhanced intermolecular interaction in the solid leads to the formation of delocalized electronic states, which manifests as broadening of the absorption bands. Using cerium and DBTTF, we have established a platform where reversible photo-induced charge transfer modulates both magnetism and conductivity. The observed reduction (over 40%) in magnetic moment upon illumination, alongside a significant increase in conductivity, highlights the potential of such hybrid systems for applications in molecular spintronics. These findings put forward molecular materials for the future development of tunable, stimuli-responsive quantum materials.

Author contributions

Synthetic work and spectroscopy characterizations were carried out by H. G. Magnetic and transport measurements were performed by H. G. and J. M. K. Computational work was performed by E. P. S., X. Y., and X. W. Elemental Analysis was performed by P. P. XANES experiment and fitting were performed by P. W. S.

The crystal structure was solved by M. R. G. The project was supervised by S. G. M., E. Z., J. A., J. M. K., and E. J. S.

Conflicts of interest

There are no conflicts to declare.

Data availability

CCDC 2495728 contains the supplementary crystallographic data for this paper.[53]

Supplementary information (SI): synthetic details, analytical data, including depictions of all spectra, magnetometry, and transport measurement details, and coordinate data of computationally optimized species, are documented in the SI. See DOI: https://doi.org/10.1039/d5sc08870d.

Acknowledgements

We gratefully acknowledge support for this work from the U.S. Department of Energy, Office of Science, Office of Basic Energy Sciences, Chemical Sciences, Geosciences and Biosciences Division, Heavy Element Chemistry Program under Award DE-SC0020169 at the University of Pennsylvania and under contract no. DE-AC02-05CH11231 at LBNL. H. G. acknowledges the Vagelos Institute for Energy Science and Technology for the graduate fellowship. H. G. also acknowledges Dr Amit Kumar for helpful discussions. E. J. S. also thanks the University of Pennsylvania for financial support. J. A. and E. Z. acknowledge the center for Computational Research (CCR, https://hdl.handle.net/10477/79221, accessed 2025/08) at U. Buffalo for providing computational resources.

Notes and references

1 L. Münzfeld, S. Gillhuber, A. Hauser, S. Lebedkin, P. Hädinger, N. D. Knöfel, C. Zovko, M. T. Gamer, F. Weigend, M. M. Kappes and P. W. Roesky, Synthesis and properties of cyclic sandwich compounds, *Nature*, 2023, **620**, 92–96.

2 M. A. Dunstan and K. S. Pedersen, Valence tautomerism, non-innocence, and emergent magnetic phenomena in lanthanide-organic tessellations, *Chem. Commun.*, 2025, **61**, 627–638.

3 J. I. Urgel, D. Écija, G. Lyu, R. Zhang, C.-A. Palma, W. Auwärter, N. Lin and J. V. Barth, Quasicrystallinity expressed in two-dimensional coordination networks, *Nat. Chem.*, 2016, **8**, 657–662.

4 T. Cheisson and E. J. Schelter, Rare earth elements: Mendeleev's bane, modern marvels, *Science*, 2019, **363**, 489–493.

5 C. H. Booth, D. Kazhdan, E. L. Werkema, M. D. Walter, W. W. Lukens, E. D. Bauer, Y.-J. Hu, L. Maron, O. Eisenstein, M. Head-Gordon and R. A. Andersen, Intermediate-Valence Tautomerism in Decamethylytterbocene Complexes of Methyl-Substituted Bipyridines, *J. Am. Chem. Soc.*, 2010, **132**, 17537–17549.

6 M. A. Dunstan, A. S. Manvell, N. J. Yutronkie, F. Aribot, J. Bendix, A. Rogalev and K. S. Pedersen, Tunable valence tautomerism in lanthanide–organic alloys, *Nat. Chem.*, 2024, **16**, 735–740.

7 T. Vitova, H. Ramanantoanina, B. Schacherl, L. Münzfeld, A. Hauser, R. S. K. Ekanayake, C. Y. Reitz, T. Prüßmann, T. S. Neill, J. Göttlicher, R. Steininger, V. A. Saveleva, M. W. Haverkort and P. W. Roesky, Photon-Modulated Bond Covalency of $[Sm(II)(\eta^9\text{-}C_9H_9)_2]$, *J. Am. Chem. Soc.*, 2024, **146**, 20577–20583.

8 E. Luneva, M. A. Dunstan, F. Aribot, N. J. Yutronkie, J. E. McPeak, A. Rogalev, G. Nocton and K. S. Pedersen, 4f-intermediate valence in an ytterbium–bipyridine coordination solid, *Chem. Commun.*, 2025, **61**, 14999–15002.

9 O. Sato, Dynamic molecular crystals with switchable physical properties, *Nat. Chem.*, 2016, **8**, 644–656.

10 A. Viborg, M. A. Dunstan, N. J. Yutronkie, A. Chanda, F. Trier, N. Pryds, F. Wilhelm, A. Rogalev, D. Pinkowicz and K. S. Pedersen, Disentangling chemical pressure and superexchange effects in lanthanide–organic valence tautomerism, *Chem. Sci.*, 2025, **16**, 6879–6885.

11 J. M. Robinson, Valence transitions and intermediate valence states in rare earth and actinide materials, *Phys. Rep.*, 1979, **51**, 1–62.

12 C. H. Booth, M. D. Walter, M. Daniel, W. W. Lukens and R. A. Andersen, Self-Contained Kondo Effect in Single Molecules, *Phys. Rev. Lett.*, 2005, **95**, 267202.

13 D.-C. Sergentu, C. H. Booth and J. Autschbach, Probing Multiconfigurational States by Spectroscopy: The Cerium XAS L3-edge Puzzle, *Chem.–Eur. J.*, 2021, **27**, 7239–7251.

14 N. Mahieu, J. Piątkowski, T. Simler and G. Nocton, Back to the future of organolanthanide chemistry, *Chem. Sci.*, 2023, **14**, 443–457.

15 P. Pandey, X. Wang, H. Gupta, P. W. Smith, E. Lapsheva, P. J. Carroll, A. M. Bacon, C. H. Booth, S. G. Minasian, J. Autschbach, E. Zurek and E. J. Schelter, Realization of Organocerium-Based Fullerene Molecular Materials Showing Mott Insulator-Type Behavior, *ACS Appl. Mater. Interfaces*, 2024, **16**, 17857–17869.

16 H. Gupta, B. D. Vincenzini, A. M. Bacon and E. J. Schelter, Assembly of a trapped valent CeIII/IV–TCNQ complex through metal–ligand redox cooperativity, *Chem. Commun.*, 2024, **60**, 6909–6912.

17 D. Jérome, Organic Conductors: From Charge Density Wave TTF–TCNQ to Superconducting $(TMTSF)_2PF_6$, *Chem. Rev.*, 2004, **104**, 5565–5592.

18 K. P. Goetz, J. Y. Tsutsumi, S. Pookpanratana, J. Chen, N. S. Corbin, R. K. Behera, V. Coropceanu, C. A. Richter, C. A. Hacker, T. Hasegawa and O. D. Jurchescu, Polymorphism in the 1:1 Charge-Transfer Complex DBTTF–TCNQ and Its Effects on Optical and Electronic Properties, *Adv. Electron. Mater.*, 2016, **2**, 1600203.

19 W. R. H. Hurtley and S. Smiles, CCXCIX.—2: 2′-Bis-1: 3-benzdithiolene, *J. Chem. Soc.*, 1926, **129**, 2263–2270.

20 O. N. Kazheva, D. M. Chudak, G. V. Shilov, A. V. Kravchenko, I. D. Kosenko, I. B. Sivaev, G. G. Abashev, E. V. Shklyaeva, V. A. Starodub, L. I. Buravov, V. I. Bregadze and

O. A. Dyachenko, First radical cation salts based on dibenzotetrathiafulvalene (DBTTF) with metallacarborane anions: Synthesis, structure, properties, *J. Organomet. Chem.*, 2020, **930**, 121592.

21 H. Yin, Y. Jin, J. E. Hertzog, K. C. Mullane, P. J. Carroll, B. C. Manor, J. M. Anna and E. J. Schelter, The Hexachlorocerate(III) Anion: A Potent, Benchtop Stable, and Readily Available Ultraviolet A Photosensitizer for Aryl Chlorides, *J. Am. Chem. Soc.*, 2016, **138**, 16266–16273.

22 B. A. Scott, F. B. Kaufman and E. M. Engler, Formation of highly conducting organic salts by photooxidation of heterofulvalene .pi.-donors in halocarbon solutions, *J. Am. Chem. Soc.*, 1976, **98**, 4342–4344.

23 T. Iwasaki, T. Sawada, M. Okuyama and H. Kamada, The photochemical reaction of aromatic amines with carbon tetrachloride, *J. Phys. Chem.*, 1978, **82**, 371–372.

24 B. Zelent and G. Durocher, One-electron photooxidation of N-ethylcarbazole in the presence of carbon tetrachloride. Products and mechanism of the photochemical reaction, *Can. J. Chem.*, 1985, **63**, 1654–1665.

25 L. L. Miller and R. S. Narang, Induced Photolysis of DDT, *Science*, 1970, **169**, 368–370.

26 M. Masson, P. Delhaes and S. Flandrois, Photooxidation of tetrathiatetracene and tetraselenatetracene in halocarbon solutions: formation of new radical-cation salts, *Chem. Phys. Lett.*, 1980, **76**, 92–95.

27 H. Shimamori and H. Musasa, Contact-Ion-Pair Formation in Photolyzed Aniline and N,N-Dimethylaniline in the Presence of CCl4, *J. Phys. Chem.*, 1996, **100**, 5343–5348.

28 Y. Ahn, J. Y. Koo and H. C. Choi, A Platform to Evaluate the Effect of Back Charge Transfer on the Electrical Conductivity of TTF Charge Transfer Complexes: TTF_3MCl_6 (M = In, Sb), *Inorg. Chem.*, 2022, **61**, 791–795.

29 Y. Kobayashi, A. Suzuki, Y. Yamada, K. Saigo and T. Shibue, Synthesis, characterization, and dc conductivity of hydrogen-bonding dibenzotetrathiafulvalene (DBTTF) based salts, *Synth. Met.*, 2010, **160**, 575–583.

30 J. Joseph, M. Berville, J. Wytko, J. Weiss and H.-P. Jacquot de Rouville, π-mers and π-dimers: Two Radical Supramolecular Interactions – A Tutorial Review, *Chem.–Eur. J.*, 2025, **31**, e202403115.

31 S. S. Batsanov, Van der Waals Radii of Elements, *Inorg. Mater.*, 2001, **37**, 871–885.

32 O. Drozdova, H. Yamochi, K. Yakushi, M. Uruichi, S. Horiuchi and G. Saito, Determination of the Charge on BEDO-TTF in Its Complexes by Raman Spectroscopy, *J. Am. Chem. Soc.*, 2000, **122**, 4436–4442.

33 Y. Lee, H. Ki, D. Im, S. Eom, J. Gu, S. Lee, J. Kim, Y. Cha, K. W. Lee, S. Zerdane, M. Levantino and H. Ihee, Cerium Photocatalyst in Action: Structural Dynamics in the Presence of Substrate Visualized via Time-Resolved X-ray Liquidography, *J. Am. Chem. Soc.*, 2023, **145**, 23715–23726.

34 S. Matsuzaki, T. Moriyama and K. Toyoda, Raman spectra of mixed valent TTF salts; relation between Raman frequency and formal charge, *Solid State Commun.*, 1980, **34**, 857–859.

35 M. Tanaka, M. Shimizu, Y. Saito and J. Tanaka, Raman spectra of radical ion DBTTF complexes; relation between raman frequency and formal charge, *Chem. Phys. Lett.*, 1986, **125**, 594–596.

36 A. Kotani, K. O. Kvashnina, S. M. Butorin and P. Glatzel, Spectator and participator processes in the resonant photon-in and photon-out spectra at the Ce L_3 edge of CeO_2, *Eur. Phys. J. B*, 2012, **85**, 257.

37 A. Kotani and H. Ogasawara, Theory of core-level spectroscopy of rare-earth oxides, *J. Electron Spectrosc. Relat. Phenom.*, 1992, **60**, 257–299.

38 H. H. Wilson, X. Yu, T. Cheisson, P. W. Smith, P. Pandey, P. J. Carroll, S. G. Minasian, J. Autschbach and E. J. Schelter, Synthesis and Characterization of a Bridging Cerium(IV) Nitride Complex, *J. Am. Chem. Soc.*, 2023, **145**, 781–786.

39 T. A. Pham, A. B. Altman, S. C. E. Stieber, C. H. Booth, S. A. Kozimor, W. W. Lukens, D. T. Olive, T. Tyliszczak, J. Wang, S. G. Minasian and K. N. Raymond, A Macrocyclic Chelator That Selectively Binds Ln^{4+} over Ln^{3+} by a Factor of 1029, *Inorg. Chem.*, 2016, **55**, 9989–10002.

40 S. G. Minasian, E. R. Batista, C. H. Booth, D. L. Clark, J. M. Keith, S. A. Kozimor, W. W. Lukens, R. L. Martin, D. K. Shuh, S. C. E. Stieber, T. Tylisczcak and X.-d. Wen, Quantitative Evidence for Lanthanide-Oxygen Orbital Mixing in CeO_2, PrO_2, and TbO_2, *J. Am. Chem. Soc.*, 2017, **139**, 18052–18064.

41 S. Hünig, G. Kießlich, H. Quast and D. Scheutzow, Über zweistufige Redoxsysteme, (X1) Tetrathio-äthylene und ihre höheren Oxidationsstufen, *Justus Liebigs Ann. Chem.*, 1973, **1973**, 310–323.

42 Y. Qiao and E. J. Schelter, Lanthanide Photocatalysis, *Acc. Chem. Res.*, 2018, **51**, 2926–2936.

43 K. Kobayashi, M. Suzuki, T. Sato, Y. Horii, T. Yoshida, B. K. Breedlove, M. Yamashita and K. Katoh, Spin dynamics phenomena of a cerium(iii) double-decker complex induced by intramolecular electron transfer, *Dalton Trans.*, 2024, **53**, 11664–11677.

44 C. Uruburo, D. M. R. Y. P. Rupasinghe, H. Gupta, R. M. Knieser, L. M. Lopez, M. H. Furigay, R. F. Higgins, P. Pandey, M. R. Baxter, P. J. Carroll, M. Zeller, S. C. Bart and E. J. Schelter, Metal–Ligand Redox Cooperativity in Cerium Amine-/Amido-Phenolate-Type Complexes, *Inorg. Chem.*, 2024, **63**, 9418–9426.

45 O. Pajuelo-Corral, M. Contreras, S. Rojas, D. Choquesillo-Lazarte, J. M. Seco, A. Rodríguez-Diéguez, A. Salinas-Castillo, J. Cepeda, A. Zabala-Lekuona and I. J. Vitorica-Yrezabal, Cerium(iii) and 5-methylisophthalate-based MOFs with slow relaxation of magnetization and photoluminescence emission, *Dalton Trans.*, 2024, **53**, 11750–11761.

46 J. D. Rinehart and J. R. Long, Exploiting single-ion anisotropy in the design of f-element single-molecule magnets, *Chem. Sci.*, 2011, **2**, 2078–2085.

47 T. Mori, Organic Conductors with Unusual Band Fillings, *Chem. Rev.*, 2004, **104**, 4947–4970.

48 M. Atzori, F. Pop, P. Auban-Senzier, R. Clérac, E. Canadell, M. L. Mercuri and N. Avarvari, Complete Series of Chiral Paramagnetic Molecular Conductors Based on

Tetramethyl-bis(ethylenedithio)-tetrathiafulvalene (TM-BEDT-TTF) and Chloranilate-Bridged Heterobimetallic Honeycomb Layers, *Inorg. Chem.*, 2015, **54**, 3643–3653.

49 T. Enoki and A. Miyazaki, Magnetic TTF-Based Charge-Transfer Complexes, *Chem. Rev.*, 2004, **104**, 5449–5478.

50 H. Cui, T. Otsuka, A. Kobayashi, N. Takeda, M. Ishikawa, Y. Misaki and H. Kobayashi, Structural, Electrical, and Magnetic Properties of a Series of Molecular Conductors Based on BDT-TTP and Lanthanoid Nitrate Complex Anions (BDT-TTP = 2,5-Bis(1,3-dithiol-2-ylidene)-1,3,4,6-tetrathiapentalene), *Inorg. Chem.*, 2003, **42**, 6114–6122.

51 Q. Yang, E. Song, Y. Wu, C. Li, M. R. Gau, J. M. Anna, E. J. Schelter and P. J. Walsh, Mechanistic Investigation of the Ce(III) Chloride Photoredox Catalysis System: Understanding the Role of Alcohols as Additives, *J. Am. Chem. Soc.*, 2025, **147**, 2061–2076.

52 R. Murase, C. F. Leong and D. M. D'Alessandro, Mixed Valency as a Strategy for Achieving Charge Delocalization in Semiconducting and Conducting Framework Materials, *Inorg. Chem.*, 2017, **56**, 14373–14382.

53 CCDC 2495728: Experimental Crystal Structure Determination, 2026, DOI: 10.5517/ccdc.csd.cc2ps0cw.